Sub-Rayleigh resolution by phase imaging

Yann Cotte,* M. Fatih Toy, Etienne Shaffer, Nicolas Pavillon, and Christian Depeursinge

Ecole Polytechnique Fédérale de Lausanne (EPFL), Advanced Photonics Laboratory, 1015 Lausanne, Switzerland

**Corresponding author: yann.cotte@a3.epfl.ch*

Received March 29, 2010; revised May 28, 2010; accepted June 7, 2010;
posted June 8, 2010 (Doc. ID 126139); published June 22, 2010

We report the experimental observation of systematically occurring phase singularities in coherent imaging of sub-Rayleigh distanced objects. A theory that relates the observation to the sub-Rayleigh distance is presented and compared with experimental measurements. As a consequence, the limit of resolution with coherent illumination is extended by a factor of 1.64×. © 2010 Optical Society of America

OCIS codes: 030.1670, 090.1995, 100.6640, 100.5070, 110.0180.

The limit of resolution is generally expressed by Rayleigh's criterion of resolution [1], given in Eq. (1) for coherent light:

$$d_{\mathrm{min,coh}} = 0.82\frac{\lambda}{\mathrm{NA}}. \tag{1}$$

Originally, Rayleigh formulated that two incoherently imaged points are resolved if the maximum of one PSF lies in the first minimum of the other PSF. Because of interference, that criterion does not apply for coherent imaging and was reformulated by Sparrow as a contrast criterion of 27% of the minimum between two maxima. Consequently, the prefactor in the case of coherent imaging is 1.34× superior to the one in the case of incoherent imaging (0.61). Thus, the imaging system illuminated by incoherent light is supposed to have inferior resolving power compared to the coherently illuminated one. Recently, the demonstrated interference of spherical waves has been theoretically deduced to generate vortex arrays [2], as anticipated by intensity measurements and computation of near fields [3]. We report a new (to our knowledge) method that states how singularities can be used for improving the coherent image resolution power. Following the idea of phase singularities created in Young's interference pattern [4], our test target consists of a thin opaque aluminum film (thickness = 100 nm) on a conventional coverslip. Instead of pinholes, nanometric apertures are drilled by focused ion beam (FIB) in the coating and are placed at very close distances d, smaller than the limit of resolution in Eq. (1). The distance is controlled and measured by scanning electron microscopy (SEM), as shown in Figs. 1(a), 1(d), and 1(g). The SEM measurements reveal slightly conical holes of $Ø_{\mathrm{real}} \approx$ 90 nm diameter. The measured center-to-center (ctc) distances d match within a precision of ±5 nm.

We demonstrated that a single nanometric aperture can be used as a complex point source [5]. In this approach, the complex field can be accessed by using digital holographic microscopy (DHM) [6] in a transmission configuration. Thus, the amplitude, as well as the phase of the complex field emitted by two closely spaced nanoholes, can be extracted by following the methods of [6,7]. The results are shown in Fig. 1 where $\mathrm{NA_{eff}}$ is determined from the phase image of a single nanometric aperture placed on the same test target.

The images show the amplitudes [cf. Figs. 1(b), 1(e), and 1(h)] of two PSFs beneath the coherent limit of resolution ($d_{\mathrm{min,exp}} = 526$ nm). It can be seen that the two PSFs converge and can no longer be distinguished by the contrast criterion. Accordingly, the phase images [cf. Figs. 1(c), 1(f), and 1(i)] show the superposition of the known concentric interference pattern of the PSF [7]. The concentric phase pattern is the result of a spherical wave varying from $-\pi$ to π. This superposition results in the generation of lines of phase singularities. Their direct observation in lateral phase images is presented for the first time, to our knowledge, as well as

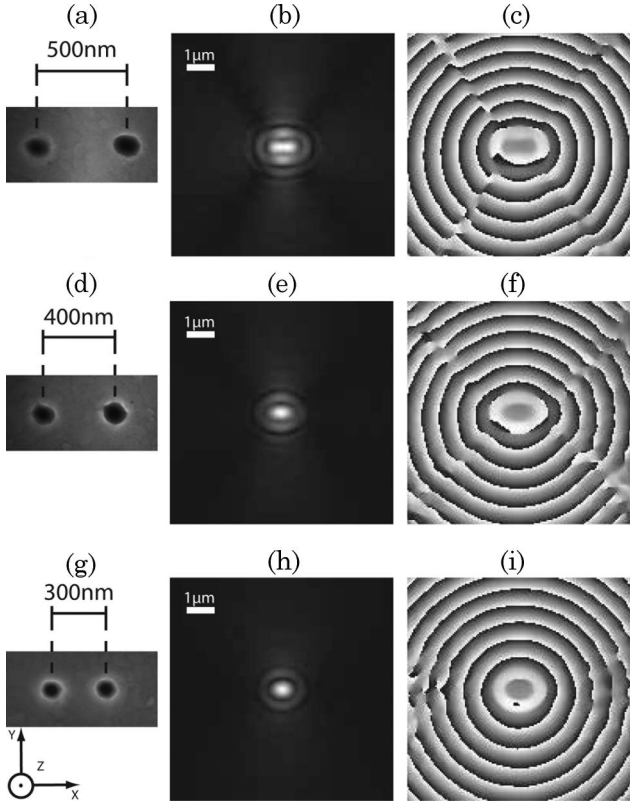

Fig. 1. Experimental SEM images of test targets (a), (d), and (g) and their experimental DHM images [(b) and (c), (e) and (f), (h) and (i)] in the focal plane for $\lambda = 532$ nm and $\mathrm{NA_{eff}} = 0.83$. The test targets are couples of nanoholes drilled by FIB in an aluminum film and are pictured at 100,000× magnification with corresponding scale bars. Respectively displayed in (b) and (c) are the imaged amplitudes and their corresponding phases of test target (a), with nanohole ctc distance $d = 500$ nm. (d)–(f) are the corresponding results for $d = 400$ nm, and (g)–(i) are for $d = 300$ nm.

a method for direct exploitation. It turns out that the direction of those lines of singularities varies systematically with the ctc distance of the two holes, as can be seen by comparing Figs. 1(c), 1(f), and 1(i).

The lines of phase singularities can be explained as the result of an interference phenomenon. The spherical waves emitted from each nanohole intercept mutually and create destructive interferences at the positions where $\Delta\Phi = \pi$. Especially in Fig. 1(c), the convergence of out-of-phase wavefronts results in singularities that can be very well observed. The phase arrangement in the focal image plane is schematically illustrated in Fig. 2, which shows the circles of equal phases with π spacings.

Considering the scale of the holes' diameter Ø_{real} of about $\lambda/6$ and their circular shape [cf. Figs. 1(a), 1(d), and 1(g)], a simple geometrical model of ideal point sources is presumed in the far field [8]. Because the considered ctc distances are above the near-field scale, higher-order scattering effects are neglected.

A total of four destructive interferences are possible for the two commutable pairs of rings, which explains the observations of Fig. 1. The characteristic spacing s between two out-of-phase circles with radii $r_1 = r$ and $r_2 = r + s$ can be calculated by

$$s = \frac{\Delta\Phi}{k_{\max}} = \frac{\pi}{(2\pi/\lambda)\text{NA}} = \frac{\lambda}{2\text{NA}}, \tag{2}$$

with the maximal spatial frequency $k_{\max}$ allowed by NA. In the event of an offset phase difference $\Delta\phi$, for instance, through a longitudinal displacement Δz, a correction $\Delta s = \lambda\Delta\phi/(2\pi)$ is introduced in $r_2 = r \pm \Delta s + s$. Hence, the effective spacing,

$$s_0 = s \pm \Delta s = s(1 \pm \text{NA}\Delta\phi/\pi), \tag{3}$$

can be contracted or dilated. Applying Pythagorus to the interception point's triangle results in

$$x^2 + (a/2)^2 = r_2^2, \qquad (d - x)^2 + (a/2)^2 = r_1^2, \tag{4}$$

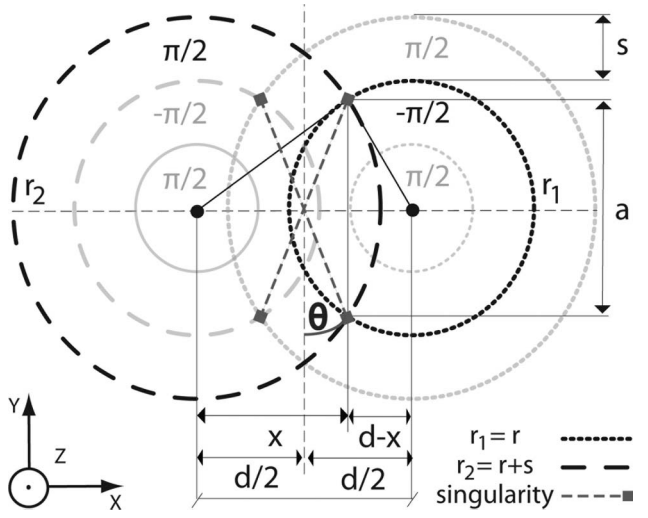

Fig. 2. Schematic illustration of image plane in phase with $\Delta\phi = 0$. Circles show contours of equal phase emitted from two point sources located the circles' center.

according to Fig. 2. Furthermore, the angle θ relative to the symmetry axis is given by the following trigonometric relation:

$$\tan\theta = \frac{x - d/2}{a/2}. \tag{5}$$

Combining the geometrical relations in Eqs. (4) and (5) and solving for d results in

$$d(\theta, r, s_0) = \{2r^2 + 2rs_0 + s_0^2 - [4r^2(r + s_0)^2 - s_0^2(2r + s_0)^2\cot^2\theta]^{1/2}\}^{1/2}. \tag{6}$$

This equation yields to symmetric singularities (cf. left and right sides in Fig. 2) if $s_0 = s$. However, a phase difference $\Delta\phi$ breaks this symmetry, in which a Δz displacement is coded. Given the examined experimental situation $\Delta\phi = 0$, though, we restrict the considerations to $s_0 = s$. The parameter r in Eq. (6) describes the dependence of θ of the order of the equal phase circle: for higher-order rings, θ will be smaller than for lower orders of the same distance d. Therefore, strictly speaking, the line of singularities is bent. To quantify this effect, Eq. (6) is plotted in Fig. 3 for different r and d values. The plot shows that the curvature is strongest for large distances d. However, the curvature (represented in light gray in Fig. 3) decreases asymptotically for smaller distances and becomes negligible. Furthermore, the scheme in Fig. 2 suggests that θ can maximally reach $\pi/2$. The minimal deducible distance, therefore, given for the maximal angle of θ, is

$$\theta_{\max} = \pi/2 \Rightarrow d_{\min} = s. \tag{7}$$

This equation states a new limit of resolution based on an adapted coherent resolution criterion. It results in resolvable distance of minimal spacing 1.64× smaller than suggested by Eq. (1), and even 1.24× superior to the corresponding equation for the incoherently illuminated case. To test this hypothesis and to verify Eq. (6), we have measured θ directly from the experimental results shown in Fig. 1 (600 nm distanced nanohole couple not

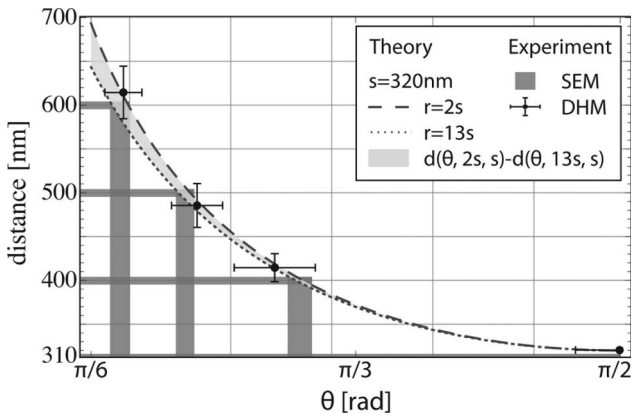

Fig. 3. Deduction of nanohole distances from angle θ of phase singularities for $\lambda = 532$ nm and $\text{NA}_{\text{eff}} = 0.83$. The line plot indicates the theoretical relation for different reference radii r. The points and gray bars indicate the experimental results from Table 1 and their corresponding ranges of trust.

Table 1. Results of Angle Measurements of Experimental Data for λ=532 nm and NA_{eff}=0.83

$FIB_{nominal}$	Distance	Error Source	Unit	600 nm	500 nm	400 nm	300 nm
SEM	$d \pm \overline{\Delta}$	reading	(nm)	600 ± 5	498 ± 5	403 ± 5	304 ± 5
DHM	$\bar{\theta} \pm \overline{\Delta\theta}$	mean reading	(degree)	31.6 ± 2.1	42.1 ± 2.9	50.9 ± 4.6	90 ± 10
With Eq. (6)	$\bar{d} \pm \overline{\sigma_d}$	mean propagated	(nm)	614 ± 30	485 ± 25	414 ± 16	≤ 320

illustrated). The results are summarized Table 1. θ_i is measured as a function of r_i for several phase contours ($N = 12$) with a reading precision of $\Delta\theta_i$ for each ctc distance. The associated hole distances d_i are calculated by Eq. (6), and their uncertainties $\sigma_{d,i}$ are determined according to the error propagation of $\Delta\theta_i$. Table 1 indicates the mean values with a precision of the error in the mean. Therefore, $\overline{\Delta\theta}$ indicates the visibility of the phase singularities, whereas $\overline{\sigma_d}$ shows how much the deduced distance is sensitive to variations of θ.

According to the uncertainties of $\bar{d}$, the lateral precision reaches ≈24 nm. The 300 nm measurement, though, is just beneath the limit of resolution in phase given by Eqs. (2) and (7). As seen in Fig. 1(i), the four singularity lines are merged to two and result in $\theta = \pi/2$. The smearing out ($\overline{\Delta\theta} = \pm 10°$) of the phase singularity in Fig. 1(i) can be interpreted as the visual limit of resolution in phase where the unique orientation of the singularity is lost. Consequently, the distance can be estimated to be 320 nm or smaller.

In Fig. 3, all experimental results of Table 1 are compared to the theoretical d–θ relationship according to Eq. (6). The deduced distances $\bar{d}$ are found to match the real ones. Vice versa, the measured angles $\bar{\theta}$ overlap with the associated θ of the real distances. The asymptotic behavior of the theoretical curve explains the trend of $\overline{\sigma_d}$ to become more accurate for bigger angles. However, this advantageous sensitivity is partially compensated by an opposed trend of $\overline{\Delta\theta}$, i.e., the singularities become less prominent for decreasing distances d. Moreover, a curvature of the lines of singularities is not visible in Figs. 1(c) and 1(f), since $\overline{\Delta\theta}$ is bigger than the variation due to the r dependence (cf. Fig. 3, light gray). Finally, the assumption of constant s may augment $\overline{\sigma_d}$ if NA_{eff} is affected by asymmetric aberrations, e.g., coma or astigmatism, which can be seen in Figs. 1(c), 1(f), and 1(i) as small variations of s in different directions.

Our results endorse the simple theoretical consideration based on the assumption that each sub-Rayleigh object acts as a spherical wave emitter according to the Huygens principle [8]. In the classical imaging formalism for incoherent light, those emitters do not interact and are simply imaged as an ensemble of PSF. Nonetheless, the coherent imaging bears the capability of recovering such intrinsic crosstalk. In this aspect, the observation of singularities can be seen as a variant of structured illumination microscopy where the structured illumination results from the sample properties themselves. The enhanced limit of resolution given by linear structured illumination [9] is consequently comparable to Eq. (2).

In conclusion, the observation of intrinsic interference phenomena in coherent imaging of sub-Rayleigh distances has been presented. The destructive interference appears as lines of singularities in phase, and their orientations have been shown to be related to the distances between the pointlike objects. The correctness of deduced Eq. (6) is endorsed by matching the angles of singularity lines with experimental distances d. This proof of principle suggests a new resolution criterion in phase, as opposed to the contrast-based Rayleigh criterion. The limit of resolution with coherent illumination is extended by a factor of 1.64× and can be reformulated as Eq. (2). We suspect that a possible offset phase difference could further improve the resolution.

The author wants to acknowledge Swiss National Science Foundation (SNSF), grant 205 320-120 118, for its financial support and the Center of MicroNano-Technology (CMI) for the cooperation on its research facilities.

References

1. M. Born and E. Wolf, *Principles of Optics*, 6th ed. (Cambridge U. Press, 1987).
2. S. Vyas and P. Senthilkumaran, Appl. Opt. **46**, 7862 (2007).
3. M. Totzeck and H. J. Tiziani, Opt. Commun. **138**, 365 (1997).
4. H. F. Schouten, G. Gbur, T. D. Visser, and E. Wolf, Opt. Lett. **28**, 968 (2003).
5. Y. Cotte and C. Depeursinge, in *Proceedings of Focus on Microscopy*, Advanced Linear and Non-Linear Imaging (2009), paper TU-AF2–PAR-D.
6. E. Cuche, P. Marquet, and C. Depeursinge, Appl. Opt. **38**, 6994 (1999).
7. A. Marian, F. Charrière, T. Colomb, F. Montfort, J. Kühn, P. Marquet, and C. Depeursinge, J. Microsc. **225**, 156 (2007).
8. X. Heng, X. Q. Cui, D. W. Knapp, J. G. Wu, Z. Yaqoob, E. J. McDowell, D. Psaltis, and C. H. Yang, Opt. Express **14**, 10410 (2006).
9. M. G. L. Gustafsson, Proc. Natl. Acad. Sci. USA **102**, 13081 (2005).